Zn(II) and Cd(II) complexes with 3-furoic acid. Exploring the role of C—H⋯O interactions

Francisco Sánchez-Férez [a],[1], Daniel Ejarque [a],[1], Teresa Calvet [b], Mercè Font-Bardia [c], Josefina Pons [a],*

[a] Departament de Química, Universitat Autònoma de Barcelona, Bellaterra 08193, Barcelona, Spain
[b] Departament de Mineralogia, Petrologia i Geologia Aplicada, Universitat de Barcelona, Martí i Franquès s/n, Barcelona 08028, Spain
[c] Unitat de Difracció de Raig-X, Centres Científics i Tecnològics de la Universitat de Barcelona (CCiTUB), Universitat de Barcelona, Solé i Sabarís, 1-3, Barcelona 08028, Spain

ARTICLE INFO

ABSTRACT

Hydrogen bond interactions implying C—H groups and *O* atoms either from carboxylate, carbonyl, or ether functionalities have been demonstrated to play a pivotal role in the packing of crystal structures. To analyze and compare their significance in metal carboxylate complexes with pyridine derivatives (dPy), we have synthesized four Zn(II) and Cd(II) compounds containing 3-furoic acid (3-FA) and two different pyridine ligands (iso-nicotinamide, isn; and 4-acetylpyridine, 4-acpy) affording two isostructural dimeric complexes [Zn(μ-3-FA)(3-FA)(isn)$_2$]$_2$ (**1**) and [Cd(μ-3-FA)(3-FA)(isn)$_2$]$_2$ (**2**), one dimeric paddle-wheel [Zn(μ-3-FA)$_2$(4-acpy)]$_2$ (**3**), and one monomer [Cd(3-FA)$_2$(4-acpy)$_2$(OH$_2$)] (**4**). Their crystal structures have been elucidated and studied in detail, showing variable coordination modes of the 3-FA ligand and different coordination numbers. The C—H⋯O interactions analysis of the four complexes in combination with their previously reported analogs with 2-furoic (2-FA) and piperonylic (HPip) acids, highlights the importance of such associations in the final crystal arrangement benefitting from cooperative effects. Finally, the photophysical properties in MeOH solution of **1**–**4** have been analyzed and their quantum yields calculated and compared.

1. Introduction

In the intricate tapestry of molecular interactions governing the crystal packing, non-covalent interactions play a pivotal role in shaping their molecular architectures. Among them, the C—H⋯O interactions are referred to as these contacts showing a distance closer to 2.6 Å, corresponding to the sum of the van der Waals (vdW) radii of H and O, and sharing the same directional nature as conventional hydrogen bonds [1,2]. Within the biological landscape, they have been identified as a prevalent cohesive interaction in proteins responsible for amino acid-base recognition and so, play a role in the modulation of gene expression [3,4]. They can even reach 50% of the average energy contribution in the formation of protein-protein assemblies. Indeed, their weaker nature makes them more suitable for processes requiring reversible associations [5]. From a structural point of view, they are characterized as either a supportive interaction of stronger associations or as an intrusive force due to their capacity to perturb the

supramolecular patterns and topologies, as for the case of the assembly of some carboxylic acids in which the disruption of infinite O—H⋯O interactions are triggered by complementary C—H⋯O associations. Thus, this has been ascribed to a relevant interaction in the rational design of drugs, and the proper prediction of their properties [6]. In particular, the occurrence of such associations involving ether functional groups has emerged as a fascinating and nuanced area of investigation since unraveling their distinct nature is crucial for a holistic comprehension of molecular recognition and self-assembly processes [7].

The early results from this topic were gathered employing activated C—H groups with chloroform as the archetypal molecule, but later was confirmed that C—H⋯O interactions could be formed even in non-activated compounds. The strength of conventional C—H⋯O interactions, only ranging between −4.0 and −16.0 kJ·mol^{-1}, is not equivalent to classical hydrogen bonds, which achieve values of −167.0 kJ·mol^{-1} and above, but cooperativity effects confer additional

---

stabilization and could support the self-assembly [8]. Indeed, even in the presence of strong hydrogen bonds, weaker interactions constrain the crystal packing [6,9]. Besides, there is a propensity of C—H groups closer to an electronegative atom such as N, to partake in these interactions, and so, polarization effects are of tantamount importance by modulating the acidity of the C—H donor atom [2]. The archetypal chloroform···acetone interaction has been quantified to −11.3 ± 0.4 kJ·mol^{-1} [10], and even sp^3 C—H groups have demonstrated the capability of forming them [11]. These interactions are relevant in stabilizing crystal packing even when longer than the sum of vdW radii of the donor and acceptor atoms [12]. Besides, DFT calculations evinced that aliphatic C—H···O interactions such as in the structure of acrylate

can provide interaction energies up to −20.0 kJ·mol^{-1}. Therefore, the association involving aromatic C—H groups, which are more acidic could achieve greater energies [13].

Among the feasible methods to characterize C—H···O interactions, aside from the ideal single crystal X-ray diffraction, the spectroscopic ones such as Raman and infrared are fruitfully applied to its recognition and identification. The formation of the C—H···O interaction causes a conjugation between their orbitals that is reflected as a weakening of the donor C—H bond, accompanied by its lengthening. This is illustrated as a redshift of the C—H stretching [14]. All these considerations suggests that C—H···O interactions can be responsible of independent structural features instead of being a merely result from geometry. Thus,
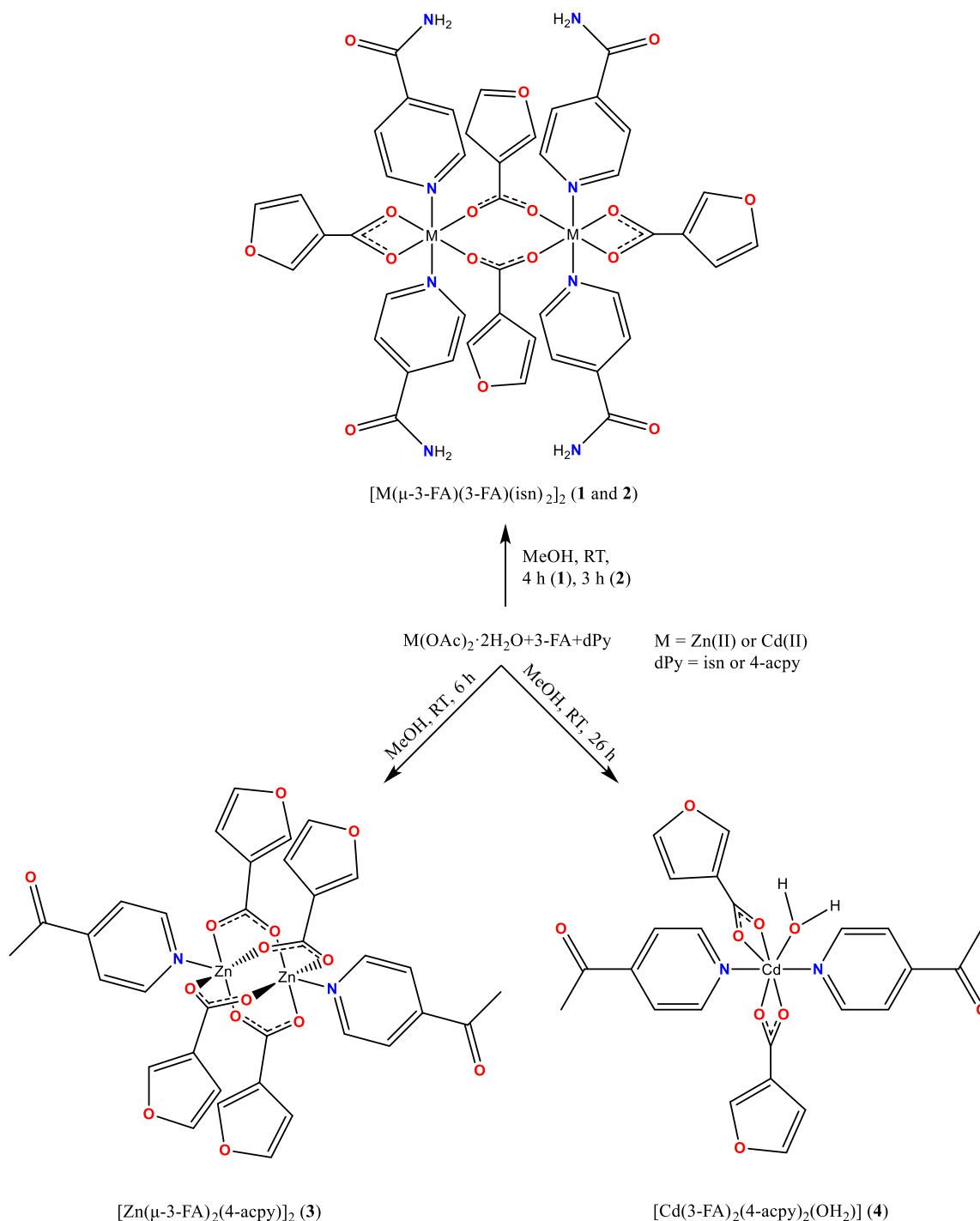
Scheme 1. Outline of the synthesis of complexes 1–4.

exploration of how C—H···O interactions contribute to the self-assembly and crystal packing of ether-, carbonyl-, and carboxylate-containing compounds, shedding light on their structural characteristics and implications, is crucial in crystal engineering and supramolecular chemistry.

Our group has been focusing on the study of both strong supramolecular synthons and weak interactions implying by studying their structure-directing effect, especially for amide-containing ligands [15]. Previous studies with piperonylic acid (HPip) evinced interactions in Zn(II) and Cd(II) complexes, or even coordination in Hg(II) complexes of the ether functionality [15,16]. Recently, we studied the five-membered ring chelation-supported coordination of the furane O atom of 2-furoic acid (2-FA) triggered by a dissolution-recrystallization structural transformation (DRST) process, which was monitored by fluorescence measurements [17,18]. Interestingly, this scenario led to highlighting the importance of the coordination ability of the furane ring, especially in solution [19]. The implications of C—H···O interactions in the arrangement of metal carboxylate complexes remain hidden, despite their importance in organic structures has been demonstrated. Therefore, to increase this knowledge, we aimed to discern interaction patterns and the supportive or intrusive behavior of C—H···O interactions in a family of ether-containing complexes, employing crystallographic data and supported by theoretical calculations. To this aim, we have performed the synthesis of two Zn(II) and two Cd(II) furoates employing the isomer of 2-FA, the 3-furoic acid (3-FA), and we kept the same dPy, 4-acpy, and isn. These reactions led to the formation of two dimers [Zn(μ−3-FA)(3-FA)(isn)$_2$]$_2$ (**1**), [Cd(μ−3-FA)(3-FA)(isn)$_2$]$_2$ (**2**), a paddle-wheel [Zn(μ−3-FA)$_2$(4-acpy)]$_2$ (**3**), and a monomer [Cd(3-FA)$_2$(4-acpy)$_2$(OH$_2$)] (**4**) (Scheme 1). Then, all this data has been compared to the aforementioned previous results with Zn(II) and Cd(II) with 2-FA [19], and to previous results with piperonylic acid (HPip) [15]. Besides, UV–Vis and fluorescence experiments were conducted to study the behavior of complexes **1–4** in solution.

2. Experimental

2.1. Synthesis of complexes 1–4

*Compounds **1** and **2**.* A MeOH solution (0.5 mL) of 3-FA (50.4 mg, 0.450 mmol) was added dropwise to a MeOH solution (0.5 mL) of M(OAc)$_2$·2H$_2$O (49.4 mg, 0.225 mmol, M = Zn(II) (**1**); 60.0 mg, 0.225 mmol, M = Cd(II) (**2**)) at room temperature (RT) under constant stirring. Then, a MeOH solution (0.75 mL (**1**), 0.50 mL (**2**)) of isn (110 mg, 0.900 mmol (**1**); 55.0 mg, 0.450 mmol (**2**)) was added dropwise to the mixture at RT, observing the immediate formation of a white precipitate, which was left under stirring for 4 h (**1**) or 3 h (**2**). The resulting powders were filtrated, washed with Et$_2$O, and dried under vacuum. Single crystals suitable for X-ray diffraction of **1** were obtained using the same methodology as for the obtention of the powder but starting from 10.1 mg of Zn(OAc)$_2$·2H$_2$O (0.0460 mmol), 10.5 mg of 3-FA (0.0937 mmol) and 21.9 mg of isn (0.179 mmol) in 1 mL of MeOH. Then, the resulting solution was left to slowly evaporate at RT for two days. Similarly, single crystals of **2** were achieved through the same methodology but starting from 10.4 mg Cd(OAc)$_2$·2H$_2$O (0.0390 mmol), 8.8 mg 3-FA (0.079 mmol) and 9.5 mg isn (0.078 mmol) in 1 mL of MeOH, and the resulting solution was left to slowly evaporate at RT for nine days. Details about the characterization of **1** and **2** are provided in the SI.

*Compounds **3** and **4**.* 4-acpy (0.166 mL, 1.50 mmol (**3**), 0.083 mL, 0.750 mmol (**4**)) was added dropwise to a MeOH solution (1 mL) of M(OAc)$_2$·2H$_2$O (82.3 mg, 0.375 mmol, M = Zn(II) (**3**), 100 mg, 0.375 mmol, M = Cd(II) (**4**)) at RT under constant stirring. Afterward, a MeOH solution (1 mL) of 3-FA (84.1 mg, 0.750 mmol) was added dropwise to the mixture. The reactions were left under stirring for 6 h (**3**) or 26 h (**4**) at RT. Then, a white powder precipitated for the reaction of **3**, which was filtered and washed with cold Et$_2$O. Differently, the reaction of **4** was cooled down in the fridge for three days until the obtention of a

white powder, which was also filtered and washed with cold Et$_2$O. Suitable crystals of **3** were obtained by recrystallization in MeOH and slow evaporation for 14 days at RT. Single crystals of **4** were directly harvested from the synthesis. Details about the characterization of compounds **3** and **4** are provided in the SI.

2.2. X-ray crystallographic data

Colorless (**1–4**) specimens were used for the X-ray crystallographic analysis. The R factor of **3** is attributed to the use of a not perfect crystal rather than a double crystal. Other attempts of crystallization were performed, but no single crystals of better quality were obtained. The X-ray intensity data were measured on a D8 Venture system equipped with a multilayer monochromator and a Mo microfocus (λ = 0.71,073 Å). For all the compounds, the frames were integrated using the Bruker SAINT software package using a narrow-frame algorithm. The structures were solved and refined using a SHELXTL Software Package (version-2018/3) [20]. Crystal data and additional details of structure refinement for **1–4** are reported in Table 1 and in the SI.

2.3. Computational details

All the ligands and solvent molecules present in the structure of the complexes containing 3-FA, 2-FA, and Pip ligands were optimized using Gaussian09 version D.01 [21] at the B3LYP/6−31G(+) level of theory [22,23]. From them, local maxima and minima of MEP were calculated and the corresponding α and β values were extracted following the reported methodology [24] using Multiwfn software [25]. MEP evaluation and graphical representation were performed with VMD software [26].

Energy framework calculations were performed with TONTO package [27], included in Crystal Explorer 17.5 [28]. For all the complexes the energy frameworks were computed at the CE-HF/3−21 G level of theory to include Cd(II) ions [29], and represented with a scale factor of 40 and a cut-off of −21 kJ·mol^{-1}. For interaction energy calculations all surrounding molecules containing at least one atom inside a 20 Å radius spherical cluster from the central molecule were considered. The threshold was set based on graphical inspection of the interaction energies which are energetically secluded into two groups combined with the evaluation of each interaction and verified from the X-ray structural data (S.I.: Fig. S1).

Lattice energies (E$_{latt}$) were computed by direct summation of interaction energies extracted from energy frameworks following the reported methodology [30,31]. Instead, for the E$_{latt}$ of the structures bearing polar space groups (P2$_1$) such as complexes **1**, **2**, [Zn(μ−2-FA)$_2$(isn)$_2$]$_2$, [Cd(μ−2-FA)$_2$(isn)$_2$]$_2$ and {[Cd(μ−2-FA)(2-FA)(OH$_2$)$_2$]$_n$[Cd(μ−2-FA)(2-FA)(4-acpy)(OH$_2$)]$_n$} [19], the cell dipole energy (E$_{cell}$) has been included [30]. To this aim, an estimated unit cell dipole moment has been calculated by summing the components along the polar direction of all molecular dipole moments in the unit cell obtained from a single point energy calculation using Gaussian09 version D.01 at the same level of theory [21]. Besides, the E$_{latt}$ of [[Cd(Pip)$_2$(isn)$_2$]$_2$·MeOH and [Cd(Pip)$_2$(4-acpy)$_2$]$_2$ bearing Z' > 1 and presenting two molecules of the same kind in the unit cell, has been computed as the average of the lattice sums for the two individual molecules.

3. Results and discussion

The synthesis and characterization of four Zn(II) and Cd(II) complexes bearing 3-FA and either isn or 4-acpy have been carried out and are presented hereafter. All the reactions were performed in MeOH at RT. Following the same trend observed in previous work with 2-FA, reactions with either Zn(II) or Cd(II) and isn ligand, resulted in the formation of two isostructural dimeric complexes (**1** and **2**). Likewise, the use of 4-acpy ligand resulted in the paddle-wheel arrangement of **3** with Zn(II) whereas the monomer **4** is formed with Cd(II) due to the

Table 1
Crystal data and structure refinement for complexes **1** – **4**.

	1	2	3	4
Empirical Formula	$C_{44}H_{36}Zn_2N_8O_{16}$	$C_{44}H_{36}Cd_2N_8O_{16}$	$C_{34}H_{26}Zn_2N_8O_{14}$	$C_{24}H_{22}CdN_2O_9$
Formula weight	1063.55	1157.61	817.31	594.83
T (K)	100(2)	100(2)	100(2)	100(2)
Wavelength (Å)	0.71073	0.71073	0.71073	0.71073
System, space group	Monoclinic, P2$_1$/c	Monoclinic, P2$_1$/c	Triclinic, P$\bar{1}$	Triclinic, P$\bar{1}$
Unit cell dimensions				
a (Å)	10.844(7)	10.9044(14)	11.635(3)	9.2833(7)
b (Å)	13.524(10)	13.5364(19)	11.638(3)	10.8396(8)
c (Å)	15.901(9)	16.135(2)	14.277(3)	13.7724(10)
α (°)	90	90	67.839(8)	105.080(3)
β (°)	103.57(2)	103.443(5)	67.107(8)	100.540(3)
γ (°)	90	90	89.990(8)	109.584(2)
V (Å^3)	2267(2)	2316.4(5)	1624.8(6)	1203.88(16)
Z	2	2	2	2
D$_{calc}$ (mg/m^3)	1.558	1.660	1.671	1.641
μ (mm^{-1})	1.140	0.999	1.554	0.964
F (000)	1088	1160	832	600
Crystal size (mm^{-3})	0.495 × 0.099 × 0.026	0.142 × 0.050 × 0.044	0.200 × 0.140 × 0.120	0.250 × 0.210 × 0.160
hkl ranges	$-15<=h<=15,-19<=k<=19,-22<=l<=22$	$-15<=h<=15,-19<=k<=19,-23<=l<=23$	$-14 \leq h \leq 16$–$14 \leq k \leq 16$$0 \leq l \leq 20$	$-13 \leq h \leq 13$–$15 \leq k \leq 15$–$19 \leq l \leq 19$
θ range (°)	2.001 to 30.608	1.920 to 30.835	1.973 to 30.268	2.126 to 30.579
Reflections collected/ unique/[R$_{int}$]	6897/6897/0.0741/ [R$_{int}$] = 0.0741	81,549/7211/0.1222/ [R$_{int}$] = 0.1222	9192/9192/ [R$_{int}$] = 0.1101	41,206/7344/ [R$_{int}$] = 0.0271
Completeness to θ (%)	100.0	100.0	99.4	99.6
Absorption correction	Semi-empirical from equivalents	Semi-empirical from equivalents	Semi-empirical from equivalents	Semi-empirical from equivalents
Max. and min. transmission	0.7461 and 0.5966	0.7461 and 0.5550	0.7459 and 0.5641	0.7461 and 0.6704
Refinement method	Full-matrix least-squares on $|F|^2$	Full-matrix least-squares on $|F|^2$	Full-matrix least-squares on $|F|^2$	Full-matrix least-squares on $|F|^2$
Data/Restrains/ Parameters	6897/1/317	7211/0/317	9192/4/411	7344/7/333
Goodness-on-fit on F^2	1.169	0.820	1.043	1.094
Final R indices [$I > 2\sigma$ (I)]	R$_1$ = 0.0363, wR$_2$ = 0.0936	R$_1$ = 0.0592, wR$_2$ = 0.1761	R$_1$ = 0.1074, wR$_2$ = 0.2458	R$_1$ = 0.0238, wR$_2$ = 0.0558
R indices (all data)	R$_1$ = 0.0373, wR$_2$ = 0.0950	R$_1$ = 0.0797, wR$_2$ = 0.2051	R$_1$ = 0.1917, wR$_2$ = 0.2849	R$_1$ = 0.0271, wR$_2$ = 0.0584
Extinction coefficient	n/a	0.0148(17)	n/a	n/a
Largest diff-peak and hole (e. Å^{-3})	2.400 and −0.427	2.232 and −1.235	1.629 and −1.770	0.678 and −0.727

coordination of a water molecule. The synthesis of the complexes has been assayed employing a 1:2:4 ratio for the Zn(II) complexes (**1** and **3**), and a 1:2:2 for those with Cd(II) (**2** and **4**).

3.1. General characterization

The four complexes have been characterized by elemental analysis (EA), FTIR-ATR, ^{1}H NMR, and ^{13}C{^{1}H} NMR spectroscopies, and single crystal X-ray diffraction. DEPT-135 experiments of one of each containing a different dPy (**2** and **4**) were also recorded.

The FTIR-ATR spectra of compounds **1** and **2** (S.I.: Figs. S2 and S3) display the characteristic ν(C = O) vibrations from the carbonyl of isn ligand at 1702 and 1697 cm^{-1}, respectively (free isn, 1655 cm^{-1}). Indeed, this vibration is sensitive to hydrogen bonds and dipole-dipole interactions [32]. Since the shift of the ν(C = O) frequency is dependent on the interactions in which partakes, and both complexes display the recurrent amide···amide homosynthon, the resulting frequency is almost identical. Besides, since N—H$_{anti}$···O between isn ligands themselves is disrupted towards the formation of a weaker N—H···O interactions with a vicinal carbonyl O atom from a 3-FA, the resulting vibrations are upfield shifted. Likewise, the ν(C = O) vibration of 4-acpy ligand can be identified at 1700 (**3**) and 1691 (**4**) cm^{-1} (S.I.: Figs. S4 and S5). In this case, the absence of strong intermolecular interactions is reflected as an almost unvaried frequency compared to the free 4-acpy (1693 cm^{-1}). In **1**, **2** and **4**, the ν(C—H)$_{ar}$ region of ∼ 3100 cm^{-1} is hindered by ν(N—H) or ν(O—H) vibrations. Besides, in **3**, where any vibration covers this region, the ν(C—H)$_{ar}$ is redshifted to lower

frequencies of 3151, 3136, and 3118 cm^{-1} compared to the free 4-acpy (3049, 3027, and 3005 cm^{-1}). This shift of almost 100 cm^{-1} is quite significant since previously reported shifts vary from 10 to 60 cm^{-1}. Thus, this shift suggests the formation of strong C—H···O interactions in **3** [14]. The carboxylate bands for ν_{as}(COO) appear at 1556 (**1**), 1554 (**2**), 1574 (**3**), and 1532 cm^{-1} (**4**) whereas bands for ν_s(COO) arise at 1419 and 1392 (**1**), 1413 and 1396 (**2**), 1421 (**3**) and 1415 cm^{-1} (**4**). The calculated Δ values (ν_{as}(COO)-ν_s(COO)) [33] were found to be 164 and 137 (**1**); 158 and 141 (**2**); 153 (**3**); 117 (**4**) cm^{-1}. These values suggest a bidentate bridged coordination mode of the 3-FA ligands (μ_2-η^1:η^1) in **1**–**3**, while in compounds **1**, **2**, and **4** a bidentate chelated (μ_1-η^2) coordination mode is inferred. Besides, for **1**–**4** aromatic rings vibrations attributable to [ν(C = C/C = N)] have been found between 1627 and 1422 cm^{-1}, while [δ(C = C/C = N)] between 1396 and 1213 cm^{-1}.

The ^{1}H and ^{13}C{^{1}H} NMR spectra were recorded in MeOH-d_4 (**1** and **2**) or dmso-d_6 (**3** and **4**). All the spectra show the signals belonging to 3-FA and either to 4-acpy or isn. In the ^{1}H NMR spectra of all the compounds, signals attributable to 3-FA protons appear between 8.02 and 6.62 ppm (S.I.: Figs. S6-S9). The signals from the aromatic protons of 4-acpy ligand appear between 8.81 and 7.82 ppm, and CH_3 protons can be found at 2.66 (**3**) and 2.62 (**4**) ppm (free 4-acpy: 8.68, 7.69 and 2.36 ppm). The aromatic signals from isn appear between 8.72 and 7.83 ppm (free isn: 8.84, 7.88 ppm) [34]. In addition, the ^{1}H NMR spectra of **1**–**4** confirm the 1:1 (**1**, **2**, and **4**), or 2:1 (**3**) molar ratio of the 3-FA with regards to 4-acpy or isn ligands.

In the ^{13}C{^{1}H} NMR spectra, the signals corresponding to the carboxylate group of the 3-FA ligands have been found at 169.5 (**1**),

169.6 (**2**), 168.6 (**3**), and 169.2 (**4**) ppm (S.I.: Figs. S10-S13), and the aromatic carbons between 150.9 and 111.0 ppm. The signals attributable to the $C=O_{isn}$ are at 172.5 (**1**) and 172.7 ppm (**2**) and those from the $C=O_{4-acpy}$ at 198.1 ppm (**3** and **4**). Besides, the ones corresponding to the -CH_3 group are found at 27.0 (**3**) and 26.9 ppm (**4**) [34]. The correct assignment of *C* aromatic atoms required the use of DEPT-135 experiments for complexes **2** and **4** (S.I.: Figs. S14 and S15).

3.2. Crystal structure of compounds 1 and 2

They crystallized in the monoclinic P2$_1$/c space group. Both compounds are isostructural consisting of discrete dimeric arrays of the type [M$_2$(CO$_2$)$_4$]−2 + 2 [35], presenting a [MO$_4$N$_2$] *core* (M = Zn(II) (**1**), Cd (II) (**2**)) composed by two pairs of μ$_2$-η^1:η^1–3-furoate and μ$_2$-η^2–3-furoate, and four monodentate (μ$_1$-η^1) isn ligands, arranging distorted octahedral geometries (S = 2.716 (**1**), 3.644 (**2**)) [36,37] (Fig. 1; S.I.: Table S1). Their bond lengths and angles are in line with those of its analogous complexes with 2-FA previously synthesized by our group [19], as well as other similar complexes [38,39] (Table 2).

The supramolecular interactions of both complexes are dominated by the strong amide···amide homosynthon between nearby isn ligands, forming supramolecular chains along the [202] (**1**) and [101] (**2**) directions. Besides, the *anti H*-atoms (H2B and H4B) and the *meta* H-atoms (H12 and H20, **1**; H12 and H18, **2**), both from isn, interact with the μ$_2$-η^2–3-FA carboxylate oxygen atoms (O5 and O4, **1**; O2 and O1, **2**), which combined with additional C—H···O associations and a π···π interaction between nearby 3-FA rings led to the final 3D networks (Fig. 2; Table 3).

3.3. Crystal structure of compound 3

It crystallizes in the triclinic, P1̄ space group and it displays a dimeric paddle-wheel structure bearing a [ZnO$_4$N] *core* (Fig. 3a). The two Zn(II) nodes exhibit a square-pyramidal geometry (S = 0.263 for Zn(1) and 0.312 for Zn(2)) [36,37]. The dimeric unit is composed of four μ$_2$-η^1:η^1 3-furoate ligands in a *syn-syn* disposition, which joins the two Zn(II) centers and two μ$_1$-η^1 4-acpy ligands.

The basal plane is formed by four oxygen atoms from the furoate ligands with bond angles between 87.5(3)° and 89.1(3)°, while the 4-acpy ligand holds the apical position (Fig. 3b; Table 4) similar to other previously reported complexes in the literature with the same [ZnO$_4$N] *core* such as [Zn$_2$(py)$_2$(Bz)$_4$] (py=pyridine, Bz=benzoic acid), [Zn$_2$(Bz)$_4$(2,5-Me$_2$pyz)]$_n$ (2,5-Me$_2$pyz=2,5-dimethylpyrazine) [40], [Zn$_2$(Bz)$_2$(4-acpy)]$_2$ [41], [Zn$_2$(4-methylbenzoate)$_4$(4-acpy)$_2$] [42]. These compounds show similar ranges of bond lengths (2.005 – 2.080 Å) and bond angles (85.59 – 159.85°).

Table 2
Bond lengths (Å) and bond angles (°) in **1** and **2**.

1		Bond lengths (Å)		
	Zn(1)-O(1)	2.0216(15)	Zn(1)-N(1)	2.1729(17)
	Zn(1)-O(2)#1	2.0282(14)	Zn(1)-N(3)	2.1592(17)
	Zn(1)-O(4)	2.1664(17)	Zn(1)···Zn(1)	3.942(2)
	Zn(1)-O(5)	2.3817(17)		
		Bond angles (°)		
	O(1)-Zn(1)-O(2)#1	118.82(7)	O(2)#1-Zn(1)-N(3)	96.75(6)
	O(1)-Zn(1)-O(4)	146.85(5)	O(4)-Zn(1)-O(5)	57.93(6)
	O(1)-Zn(1)-O(5)	89.22(6)	O(4)-Zn(1)-N(1)	85.34(5)
	O(1)-Zn(1)-N(1)	87.52(6)	O(4)-Zn(1)-N(3)	90.13(5)
	O(1)-Zn(1)-N(3)	92.42(6)	O(5)-Zn(1)-N(1)	84.93(5)
	O(2)#1-Zn(1)-O(4)	93.63(6)	O(5)-Zn(1)-N(3)	86.60(5)
	O(2)#1-Zn(1)-O(5)	151.45(4)	N(1)-Zn(1)-N(3)	171.54(5)
	O(2)#1-Zn(1)-N(1)	90.68(6)		
2		Bond lengths (Å)		
	Cd(1)-O(1)	2.452(3)	Cd(1)-N(1)	2.334(3)
	Cd(1)-O(2)	2.339(3)	Cd(1)-N(3)	2.339(4)
	Cd(1)-O(4)	2.216(3)	Cd(1)··· Cd(1)	3.8259(6)
	Cd(1)-O(5)#1	2.227(3)		
		Bond angles (°)		
	O(1)-Cd(1)-O(2)	54.91(9)	O(2)-Cd(1)-N(3)	84.62(11)
	O(1)-Cd(1)-O(4)	89.54(10)	O(4)-Cd(1)-O(5)#1	123.60(12)
	O(1)-Cd(1)-O(5)#1	145.77(10)	O(4)-Cd(1)-N(1)	92.38(11)
	O(1)-Cd(1)-N(1)	87.15(11)	O(4)-Cd(1)-N(3)	87.71(12)
	O(1)-Cd(1)-N(3)	84.53(11)	O(5)#1-Cd(1)-N(1)	98.64(11)
	O(2)-Cd(1)-O(4)	144.15(11)	O(5)#1-Cd(1)-N(3)	88.20(12)
	O(2)-Cd(1)-O(5)#1	91.15(10)	N(1)-Cd(1)-N(3)	171.68(12)
	O(2)-Cd(1)-N(1)	90.48(11)		

1 and **2**. #1:-x + 1,-y + 2,-z + 1

The supramolecular expansion is promoted mainly by C—H···O interactions between 4-acpy and 3-FA ligands, both acting as C—H donors and *O* acceptors within the crystal structure (Table 5). The hydrogen atom (H$_9$) of the 3-FA interacts with the oxygen atom of the carbonyl group (O13) from 4-acpy ligand assembling paddle-wheel units along [101] direction. In the same way, the hydrogen atom (H34B) of the methyl group from 4-acpy interacts with the oxygen atom (O6) from the furane ring within the [001] direction, both interactions generate a layer in (33$\bar{1}$). The 3D expansion is promoted by C—H···π interactions between a hydrogen atom (H19) of the 3-FA and furoate rings along the [010] direction (Fig. 4).

3.4. Crystal structure of compound 4

It belongs to the triclinic P1̄ space group and has a monomeric structure with a [CdO$_5$N$_2$] *core* composed of two μ$_1$-η^2 3-furoate ligands, two μ$_1$-η^1 4-acpy, and one μ$_1$-η^1 water molecules (Fig. 5a).
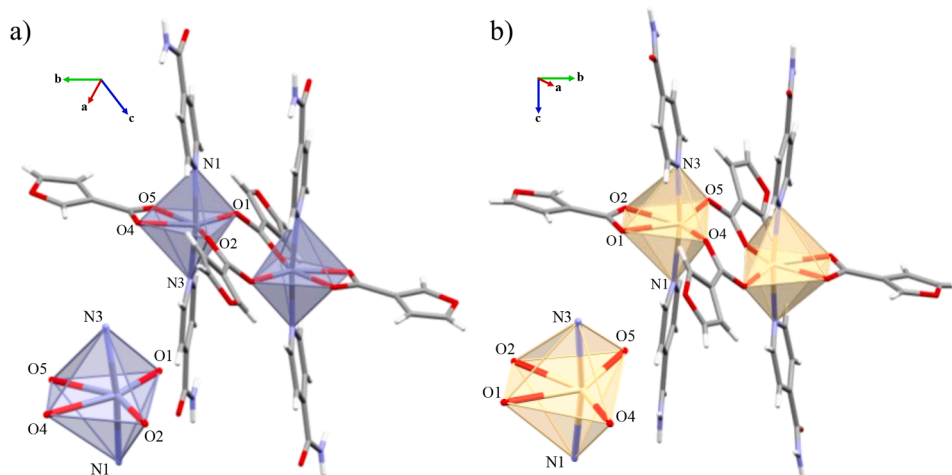
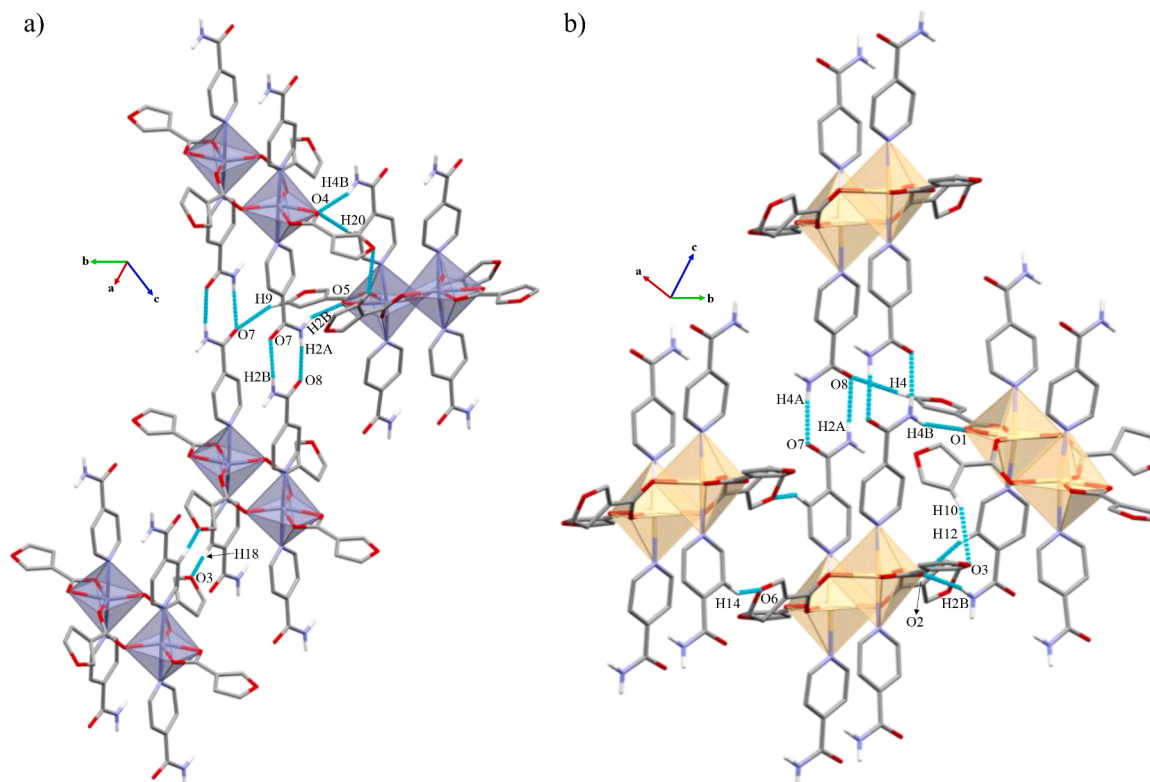**Fig. 1.** Molecular structure of compounds (a) **1** and (b) **2**.

Fig. 2. Supramolecular expansion of (a) **1** and (b) **2**. Hydrogen atoms not involved in the intermolecular interactions have been omitted for clarity.

Table 3
Intermolecular interactions present in **1** and **2**.

1	D-H···A	D-H (Å)	H···A (Å)	D···A (Å)	>D-H···A (°)	
	N(2)-H(2A)···O(8)	0.88	1.96	2.838(3)	172	
	N(2)-H(2B)···O(5)	0.88	2.02	2.848(3)	155	
	N(4)-H(4A)···O(7)	0.88	2.08	2.953(3)	171	
	N(4)-H(4B)···O(4)	0.88	2.03	2.874(3)	161	
	C(20)-H(20)···O(4)	0.95	2.36	3.288(3)	166	
	C(18)-H(18)···O(3)	0.95	2.51	3.322(4)	143	
	C(9)-H(9)···O(7)	0.95	2.40	3.151(3)	136	
	C(12)-H(12)···O(5)	0.95	2.64	3.489(3)	149	
			$\pi \cdot\cdot\pi$ interactions			
Cg(I)···Cg(J)		Cg···Cg[a]	α[b]	β, γ[c]	Cg(I)_Perp, Cg(J)_Perp[d]	Slippage[e]
Cg(1)···Cg(1)		3.568	0.00(11)	23.0	3.2851(8)	1.392
2	D-H···A	D-H (Å)	H···A (Å)	D···A (Å)	>D-H···A (°)	
	N(2)-H(2A)···O(8)	0.88	2.05	2.918(4)	169	
	N(2)-H(2B)···O(2)	0.88	2.02	2.871(4)	163	
	N(4)-H(4A)···O(7)	0.88	1.96	2.838(5)	172	
	N(4)-H(4B)···O(1)	0.88	2.02	2.843(4)	155	
	C(12)-H(12)···O(2)	0.95	2.32	3.252(4)	167	
	C(4)-H(4)···O(8)	0.95	2.37	3.156(6)	140	
	C(14)-H(14)···O(6)	0.95	2.45	3.226(6)	139	
	C(18)-H(18)···O(1)	0.95	2.63	3.499(6)	152	
			$\pi \cdot\cdot\pi$ interactions			
Cg(I)···Cg(J)		Cg···Cg[a]	α[b]	β, γ[c]	Cg(I)_Perp, Cg(J)_Perp[d]	Slippage[e]
Cg(2)···Cg(2)		3.594(3)	0.0(2)	24.5	3.2702(17)	1.490

[a] Cg···Cg = distance between ring centroids given in Å
aCg···Cg = distance between ring centroids (Å).
[b] α= dihedral angle between Planes I and J (°).
[c] Offset angles: β = angle Cg(I)-Cg(J) and normal to plane I (°) and γ = angle Cg(I)-Cg(J) and normal to plane J (°) (β = γ, when α = 0).
[d] Perpendicular distance (Å) of Cg(I) on plane J and perpendicular distance (Å) of Cg(J) on plane I (equal when α = 0).
[e] Slippage = Horizontal displacement or slippage between Cg(I) and Cg(J) (equal for both centroids when α = 0). Cg(1) = O(6)-C(7)-C(8)-C(9)-C(10); Cg(2) = O(3)-C(2)-C(3)-C(4)-C(5).

The Cd(II) ion exhibits a distorted pentagonal bipyramidal geometry (S = 2.559) [36,37], in which the equatorial plane is set by two 3-furoate ligands and one H_2O molecule (angles ranging from 53.70° to 85.49°), while the remaining 4-acpy ligands hold the axial positions (Fig. 5b,

Table 6). Bond lengths and angles are comparable to other Cd(II) compounds with similar [CdO_5N_2] *core* such as [Cd(Bz)$_2$(4-acpy)$_2$]$_2$ [41], [Cd(FB)$_2$(isn)$_2$(H_2O)]·H_2O (FB=4-formylbenzoate) [43], [Cd(μ-Pip)(Pip)(4-acpy)]$_2$ or [Cd(μ-Pip)(Pip)(isn)]$_2$ [15].
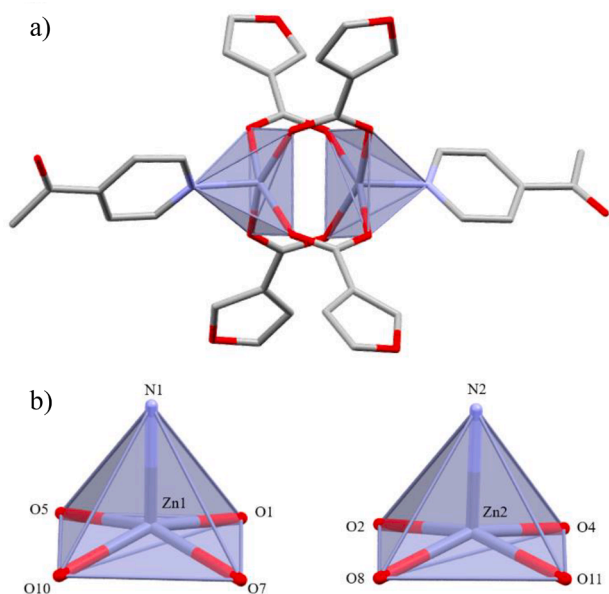
Fig. 3. (a) Molecular structure of compound **3**. (b) Coordination environment around the Zn(II) center. Hydrogen atoms have been omitted for clarity.

Table 4
Bond lengths (Å) and bond angles (°) in **3**.

Bond length (Å)			
Zn(1)-N(1)	2.011(5)	Zn(2)-N(2)	2.010(9)
Zn(1)-O(1)	2.026(5)	Zn(2)-O(8)	2.024(6)
Zn(1)-O(10)	2.029(5)	Zn(2)-O(4)	2.034(6)
Zn(1)-O(5)	2.067(7)	Zn(2)-O(11)	2.067(6)
Zn(1)-O(7)	2.091(7)	Zn(2)-O(2)	2.083(6)
Zn(1)-Zn(2)	2.934(18)		
Bond Angle (°)			
N(1)-Zn(1)-O(1)	100.56(2)	N(2)-Zn(2)-O(8)	99.09(3)
N(1)-Zn(1)-O(10)	99.56(2)	N(2)-Zn(2)-O(4)	101.24(3)
O(1)-Zn(1)-O(10)	159.88(3)	O(8)-Zn(2)-O(4)	159.67(3)
N(1)-Zn(1)-O(5)	99.45(3)	N(2)-Zn(2)-O(11)	96.29(3)
O(1)-Zn(1)-O(5)	87.47(3)	O(8)-Zn(2)-O(11)	90.21(3)
O(10)-Zn(1)-O(5)	89.13(3)	O(4)-Zn(2)-O(11)	87.20(3)
N(1)-Zn(1)-O(7)	99.62(3)	N(2)-Zn(2)-O(2)	102.36(3)
O(1)-Zn(1)-O(7)	89.02(2)	O(8)-Zn(2)-O(2)	87.86(2)
O(10)-Zn(1)-O(7)	87.79(3)	O(4)-Zn(2)-O(2)	88.19(2)
O(5)-Zn(1)-O(7)	160.93(3)	O(11)-Zn(2)-O(2)	161.32(3)
N(1)-Zn(1)-Zn(2)	179.51(17)	N(2)-Zn(2)-Zn(1)	176.20(2)
O(1)-Zn(1)-Zn(2)	79.41(2)	O(8)-Zn(2)-Zn(1)	79.86(2)
O(10)-Zn(1)-Zn(2)	80.48(2)	O(4)-Zn(2)-Zn(1)	79.83(2)
O(5)-Zn(1)-Zn(2)	81.04(2)	O(11)-Zn(2)-Zn(1)	80.09(2)
O(7)-Zn(1)-Zn(2)	79.90(2)	O(2)-Zn(2)-Zn(1)	81.28(2)

The supramolecular expansion is promoted by H-bonds, $\pi\cdots\pi$ and C—H$\cdots$O interactions (Table 6). The H-bonds are formed between the water molecule (H9OB) and one of the carboxylate O atoms from the 3-FA (O1), assembling the monomeric units along [100] direction. Besides, C—H$\cdots$O interactions support the formation of chains in this direction. The presence of $\pi\cdots\pi$ interactions between the rings of the 3-furoate, and C—H$\cdots$O interactions supporting them, generates the (001) plane (Fig. 6). Finally, the association between the carbonyl group of one 4-acpy (O7) and one of the hydrogen atoms of the other 4-acpy (H19) connects the 2D layers, forming the 3D network.

3.5. Structural role of C-H···O interactions

Herein, the effect of the acceptor ability of three different ligands (3-FA, 2-FA, HPip) on the formation of C—H$\cdots$O interactions has been analyzed through α and β values of the free ligands (S.I.: Fig. S16), and the energetics of these interactions have been quantified by energy frameworks calculations (Fig. 7, S.I.: Figs. S17 and S18). To this aim, we have selected the structures of 12 complexes containing either a furane or a dioxole ring, combined with isn and 4-acpy. The α values from the greatest donor atom, the O—H functionality of 3-FA, 2-FA, and HPip, as well as the β values of the pyridyl N atom from the dPy ligands, have been omitted since are capped to partake in intermolecular interactions after coordination. As aforementioned, the tendency to participate in C—H$\cdots$O interactions is highly influenced by the acidity of the C—H group, which is strongly related to polarization effects. Thus, α values provide a straightforward way to evaluate this acidity, in which values of ≤ 0.20 resemble remarkably weak donors [44]. Recent studies have shown that Zn(II) ions withdraw electron density from N- and O-donor ligands [45]. After coordination, this polarization should not be significantly altered but even less for *meta* position. Thus, the tendency of α and β values calculated from the free ligands could predict interactions resembling Etter's rule in which electrostatic intermolecular interactions are preferred between the best donor/best acceptor pair [46, 47]. As listed in the S.I.: Table S2, C—H groups from 3-FA are slightly more acidic than those from 2-FA or Pip ligands. Likewise, C—H groups from dPy are slightly more acidic than those from the carboxylic acids. For isn, the significantly bigger α value of C—H$_{meta\text{-isn}}$ is caused by complementarity with the N—H$_{anti}$ from the amide functionality.

Energy frameworks. The energy frameworks representation displays that all the dimeric complexes either with isn or 4-acpy adopt pillared frameworks (Fig. 7a and 7b, S.I.: Figs. S17a, S17b, S18a-c) and thus, the general packing seems to be guided by the molecular arrangement, which defines a preferred orientation of the functional groups. Besides, the presence of strong supramolecular synthons in isn complexes results in highly dimensional arrangements with tantamount interactions in all the crystallographic directions whereas dimers with 4-acpy have different interactions better understood as 2D layers with

Table 5
Intermolecular interactions present in **3**.

Intermolecular Interactions			H···A (Å)	D···A (Å)	D-H (Å)	>D-H···A (°)
C(9)-H(9)···O(13)			2.45	3.36(2)	0.950	158.8
C(34)-H(34A)···O(6)			2.59	3.48(1)	0.950	151.7
			$\pi\cdots\pi$ interactions			
Cg(I)···Cg(J)	Cg···Cg[a]	α[b]	β, γ[c]	Cg(I)_Perp, Cg(J)_Perp[d]		Slippage[e]
Cg(1)···Cg(2)	3.532(6)	4.5(6)	22.1, 17.7	3.364(5), 3.271(2)		1.330
Cg(3)···Cg(4)	3.473(7)	6.0(6)	20.2, 14.5	3.364(5), 3.260(4)		1.196
Cg(2)···Cg(5)	3.482(5)	3.9(5)	21.4, 17.6	3.320(4), 3.241(2)		1.273

[a] Cg···Cg = distance between ring centroids given in Å
  aCg···Cg = distance between ring centroids (Å).
[b] α= dihedral angle between Planes I and J (°).
[c] Offset angles: β = angle Cg(I)-Cg(J) and normal to plane I (°) and γ = angle Cg(I)-Cg(J) and normal to plane J (°) ($\beta = \gamma$, when $\alpha = 0$).
[d] Perpendicular distance (Å) of Cg(I) on plane J and perpendicular distance (Å) of Cg(J) on plane I (equal when $\alpha = 0$).
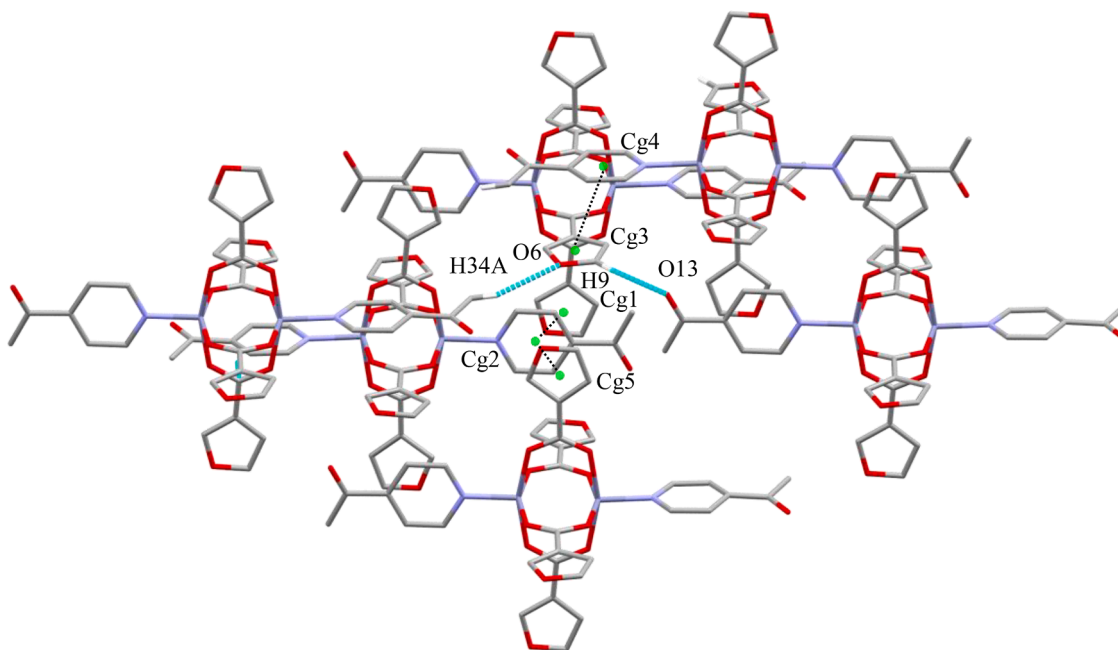[e] Slippage = Horizontal displacement or slippage between Cg(I) and Cg(J) (equal for both centroids when $\alpha = 0$). Cg(1) = O3-C2-C3-C4-C5; Cg(2) = N1-C21-C22-C23-C24-C25; Cg(3) = O9-C12-C13-C14-C15; Cg(4) = N2-C28-C29-C30-C31-C32; Cg(5) = O12-C17-C18-C19-C20.

Fig. 4. Representation of the π···π and C—H···O interactions between 4-acpy and 3-FA in **3**. Hydrogen atoms not involved in the supramolecular interactions have been omitted for clarity.
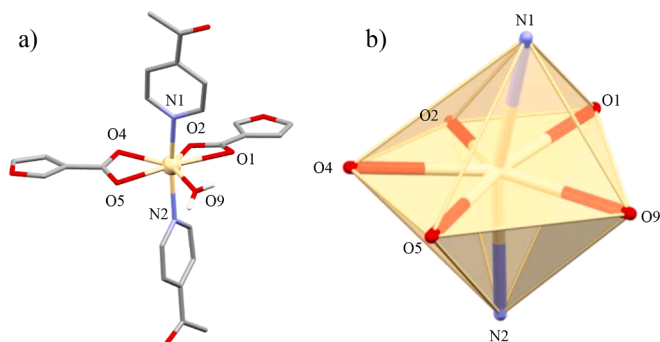
Fig. 5. (a) Molecular structure of compound **4**. (b) Coordination environment around the Cd(II) center. Hydrogen atoms are omitted for clarity.

additional weak interactions to achieve the 3D net (S.I.: S18c and S18d). Then, paddle-wheel or monomeric arrays display less ordered frameworks (Fig. 7c and 7d, S.I.: Fig. S17c and 17d). Within this set of complexes C—H···O interactions display a supportive character benefitting from cooperativity with N—H···O, O—H···O and π···π interactions. Only in those complexes without strong supramolecular synthons, the C—H···O associations provide an increase of dimensionality (1D chains for **3**, and 2D layers for **4**, [Zn(2-FA)$_2$(4-acpy)]$_2$, and [Zn(Pip)$_2$(4-acpy)]$_2$).

Association energies. Complexes **1** and **2** are composed of 3-FA and isn ligands with the greatest α values following the order N—H$_{anti}$ + C—H$_{meta}$ (3.2), N—H$_{syn}$ (2.5) both from isn, or the C—H$_{ortho-3-FA}$ (1.4). The β values are ordered starting from the carbonyl O atoms (6.1, isn; 4.8, 3-FA), and then the O furane (2.0) (S.I.: Table S2). Thus, following Etter's rule, but considering that the reciprocal amide···amide interaction is ubiquitous and almost present in all its supramolecular structures, the primary interaction for **1** and **2** should be the N—H$_{syn}$ → O=C pair, which indeed is the one displaying greater interaction energies of −217.2 (**1**) and −215.3 (**2**) kJ·mol^{-1} (S.I.: Table S3). Then, greater interaction energies are provided from cooperative C—H···O associations between the remaining functionalities. The N—H$_{anti}$ combines with

C—H$_{meta-isn}$ to interact with the carbonyl O atom of 3-FA with interaction energies of −175.7 (**1**) and −175.6 (**2**) kJ·mol^{-1} whereas the other C—H$_{meta-isn}$ is associated with the furane O atom (Figs. 1a and 1b), combined with π···π interaction to achieve interaction energy of −62.7 kJ·mol^{-1} (**1** and **2**). Complex **3** displays two C—H···O interactions, acting the two groups with the greatest α values as donors, the C—H$_{meta}$ and the -CH$_3$ from 4-acpy, and the two functionalities (O=C) with greater β values as acceptors, either from 4-acpy or 3-FA (Fig. 4). Both cooperative C—H···O associations are also combined with π···π interaction to present energies of −104.5 and −134.8 kJ·mol^{-1}. Interestingly, the furane O atom is able to act as an acceptor in a -CH$_3$···O$_{3-FA}$ association with an interaction energy of −29.7 kJ·mol^{-1}, combining the greatest donor (α = 1.5) with the greatest available O acceptor (β = 2.0). Therefore, the supramolecular assembly of **1–3** follows Etter's rule. Likewise, compound **4** also presents the aforementioned interactions, being the -CH$_3$ and CH$_{meta}$ from 4-acpy the main donors, but the presence of a coordinated water molecule generates strong O—H$_{water}$···O=C$_{3-FA}$ associations of −199.5 and −201.9 kJ·mol^{-1} that promotes the formation of a C-H$_{ortho}$···O=C$_{3-FA}$ interaction, by bringing together the monomeric units and orientating the carboxylate O atoms towards the C—H group in *ortho* position.

In the complexes containing 2-FA, those with isn [Zn(μ−2-FA)$_2$(isn)$_2$]$_2$ and [Cd(μ−2-FA)$_2$(isn)$_2$]$_2$, the greatest donors, the N—H$_{anti}$+C—H$_{meta}$ (3.2) from isn and C—H$_{ortho-2-FA}$ (1.5), combine with the best acceptors, the O = C from 2-FA (5.6) achieving interaction energies of 178.7 and 180.3 kJ·mol^{-1}, respectively (S.I.: Table S3). Then, complex [Zn(μ−2-FA)$_2$(4-acpy)]$_2$ displays C—H···O interactions from the three best donors, the -CH$_3$ (1.5) from 4-acpy and the C—H$_{ortho}$ and C—H$_{meta}$ (1.3) from 2-FA with the O = C from 4-acpy (5.0). Finally, there are two additional C—H···O interactions between the -CH$_3$ and the O furane atom from 2-FA. Indeed, probably induced by the less available position of the O furane atom, the combination of CH$_{3-4-acpy}$···O$_{2-FA}$ and C—H$_{meta-2-FA}$···O=C$_{4-acpy}$ only provides -26.5 kJ·mol^{-1}. Likewise, in [Cd(2-FA)$_2$(4-acpy)$_2$(OH$_2$)] the presence of a coordinated water molecule provide O—H···O interactions of −221.7 kJ·mol^{-1}, and the prevalent C—H···O interaction is the CH$_{3-4-acpy}$···O=C$_{3-FA}$ association. In this case, the O furane remains without interacting, and instead, a more energetically favorable CH$_{3-4-acpy}$···π$_{2-FA}$ association of −42.9 kJ·mol^{-1} is preferred.

Table 6

Bond lengths (Å), bond angles (°) and intermolecular interactions in **4**.

Bond length (Å)			
Cd(1)-O(2)	2.307(12)	Cd(1)-N(2)	2.373(14)
Cd(1)-O(9)	2.310(12)	Cd(1)-O(5)	2.504(12)
Cd(1)-O(4)	2.333(12)	Cd(1)-O(1)	2.568(12)
Cd(1)-N(1)	2.343(13)		

Bond Angle (°)			
O(2)-Cd(1)-O(9)	135.44(5)	O(9)-Cd(1)-O(5)	85.49(4)
O(2)-Cd(1)-O(4)	84.67(4)	O(4)-Cd(1)-O(5)	54.25(4)
O(9)-Cd(1)-O(4)	139.58(4)	N(1)-Cd(1)-O(5)	92.13(4)
O(2)-Cd(1)-N(1)	101.84(5)	N(2)-Cd(1)-O(5)	86.83(4)
O(9)-Cd(1)-N(1)	84.31(5)	O(2)-Cd(1)-O(1)	53.70(4)
O(4)-Cd(1)-N(1)	92.89(5)	O(9)-Cd(1)-O(1)	83.41(4)
O(2)-Cd(1)-N(2)	87.69(5)	O(4)-Cd(1)-O(1)	136.71(4)
O(9)-Cd(1)-N(2)	82.46(5)	N(1)-Cd(1)-O(1)	85.61(4)
O(4)-Cd(1)-N(2)	97.16(5)	N(2)-Cd(1)-O(1)	92.87(4)
N(1)-Cd(1)-N(2)	166.77(5)	O(5)-Cd(1)-O(1)	168.84(4)
O(2)-Cd(1)-O(5)	137.36(4)		

Intermolecular Interactions			
	H···A (Å)	D···A (Å)	D-H (Å)	>D-H···A (deg)
O(9)-H(9OA)···O(5)	1.939(18)	2.730(2)	0.794(19)	174(2)
O(9)-H(9OB)···O(1)	1.919(2)	2.741(2)	0.823(2)	175(2)
C(14)-H(14)···O(2)	2.559	3.463(3)	0.950	159.0
C(8)-H(8)···O(7)	2.526	3.475(2)	0.950	176.6
C(11)-H(11)···O(1)	2.459	3.239(2)	0.950	139.2
C(15)-H(15)···O(6)	2.493	3.243(3)	0.950	135.9
C(17)-H(17A)···O(2)	2.443	3.276(3)	0.980	142.6

π···π interactions					
Cg(I)···Cg(J)	Cg···Cg[a]	α[b]	β, γ[c]	Cg(I)_Perp, Cg(J)_Perp[d]	Slippage[e]
Cg(1)···Cg(2)	3.5750(15)	1.58(15)	22.0, 21.2	3.3336(12), 3.3153(10)	1.338
Cg(2)···Cg(1)	3.5750(15)	1.58(15)	21.2, 22.0	3.3153(10), 3.3336(12)	1.291
Cg(2)···Cg(2)	3.5160(14)	0.00(14)	21.4, 17.6	3.3612(10)	1.032

Cg(1) = 0(3)-C(2)-C(3)-C(4)-C(5); Cg(2) = O(6)-C(7)-C(8)-C(9)-C(10). [a]Cg···Cg = distance between ring centroids (Å).

[b] α= dihedral angle between Planes I and J (°).

[c] Offset angles: β = angle Cg(I)-Cg(J) and normal to plane I (°) and γ = angle Cg(I)-Cg(J) and normal to plane J (°) (β = γ, when α = 0).

[d] Perpendicular distance (Å) of Cg(I) on plane J and perpendicular distance (Å) of Cg(J) on plane I (equal when α = 0).

[e] Slippage = Horizontal displacement or slippage between Cg(I) and Cg(J) (equal for both centroids when α = 0).

Then, we analyzed complexes with Pip ligand. In [Zn(μ-Pip)(Pip) (Isn)$_2$]$_2$·2[Zn(Pip)$_2$(HPip)(Isn)]·2MeOH two isolated C—H···O interactions are present, the C—H$_{meta}$-isn···O=C$_{isn}$ with an energy of -22.3 kJ·mol^{-1} and the O—H$_{MeOH}$···O$_{Pip}$ of −29.6 kJ·mol^{-1} (S.I.: Table S3).
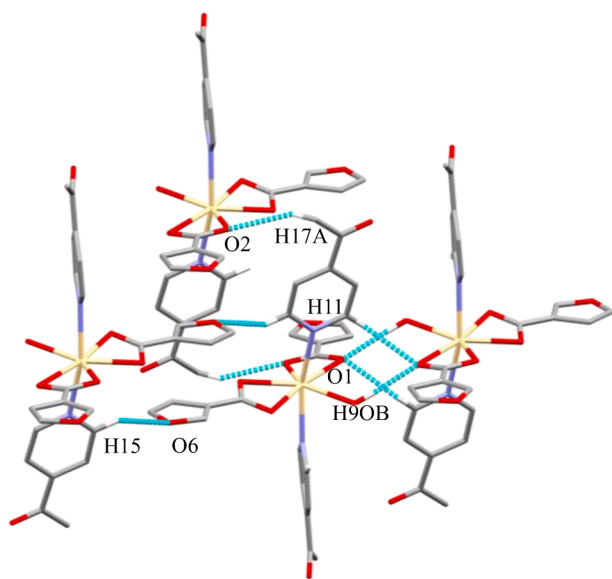
Fig. 6. Supramolecular structure of **4**. Hydrogen atoms not involved in the intermolecular interactions have been omitted for clarity.

Instead, in [Cd(μ-Pip)(Pip)(isn)$_2$]$_2$·MeOH the MeOH molecule promotes a reciprocal N—H$_{anti}$···O$_{MeOH}$ interaction of -44.20 kJ·mol^{-1} and as expected from α and β values a C—H$_{meta}$-isn···O=C$_{isn}$ association can be found with an interaction energy of −39.0 kJ·mol^{-1}. Besides the more acidic -CH$_2$ group associates Pip ligands between themselves through combination of π···π and CH$_2$···O=C$_{Pip}$ associations of −77.6 and −71.6 kJ·mol^{-1}. In [Zn(μ-Pip)$_2$(4-acpy)]$_2$ the best donor from Pip, the -CH$_2$, interacts with the O = C from 4-acpy as mentioned for the isn analog and there is also an isolated interaction of −22.2 kJ·mol^{-1} between C—H$_{meta}$-Pip···O$_{Pip}$. Complex [Cd(μ-Pip)(Pip)(4-Acpy)$_2$]$_2$ presents two C—H···O interactions with the dioxole, one is the combination of CH$_{2-Pip}$···O=C$_{4-acpy}$ and C—H$_{ortho}$-Pip···O$_{Pip}$ displaying an energy of −59.4 kJ·mol^{-1} whereas an isolated CH$_{3-4-acpy}$···O$_{Pip}$ interaction showed an interaction energy of −20.3 kJ·mol^{-1}. Finally, the difference between isn and 4-acpy complexes bearing the same dimeric arrangement, which display donor-acceptor interactions between the same ligands, can be attributable to the similar β value of the carbonyl group of HPip (5.1) and 4-acpy (5.0), whereas isn presents a greater value of 6.1. Therefore, complexes with Pip also follow Etter's rule.

Interestingly, the interactions presented strengths following the trend determined by Etter's rule from α and β values. The better C—H donors are the dPy which appear as blue-filled squares (■) combined with those interactions that mix C—H donors from dPy and C—H from the 3-FA/2-FA/Pip ligands, represented as orange-filled squares (■), and followed by pyridine-pyridine (■) and acid-acid (■) interactions (Fig. 8).

From the isolated C—H···O it is inferred that the strongest interaction energy of -44.8 kJ·mol^{-1} (○) is indeed, the association between the greater α and β pair, the CH$_2$···O = C$_{4-acpy}$ interaction. It is also foreseeable that C—H···O interactions implying aromatic groups and
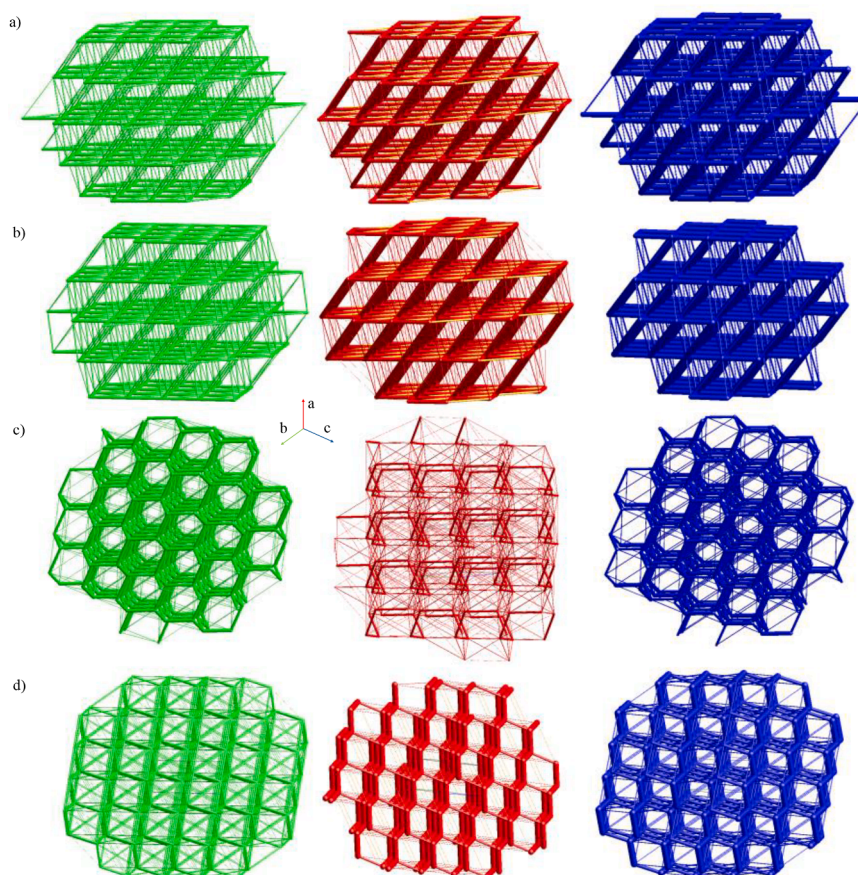
Fig. 7. Energy frameworks of complexes (a) **1**; (b) **2**; (c) **3**, and (d) **4**. In green dispersion energy (E_{disp}), in red coulombic energy (E_{cou}), and in blue total energy (E_{tot}).
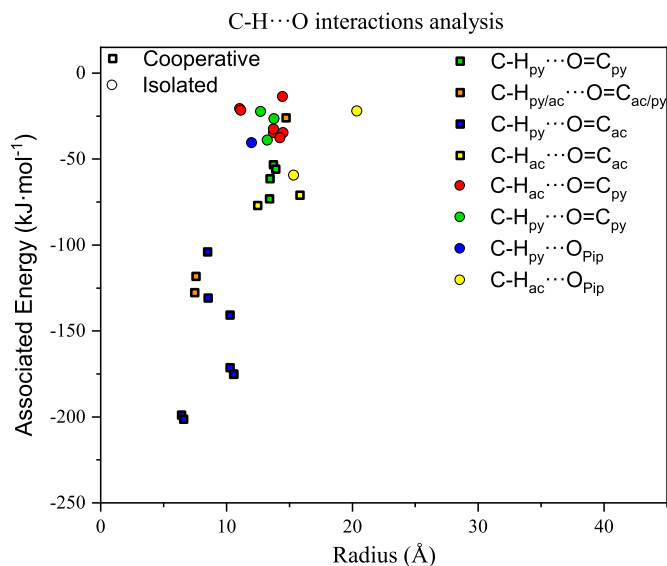

Fig. 8. Distribution of the C—H···O— interactions energies of the twelve complexes. ac stands for the carboxylates, 3-FA, 2-FA and Pip; and py stands for both dPy, isn and 4-acpy. Isolated interactions are represented as circles whereas cooperative interactions are displayed as squares, both filled with the corresponding color.

carboxylate O atoms present greater energies than those implying the ether O atoms as predicted by α and β values.

From the interaction analysis, it is clear that C—H···O are key in the crystal packing of complexes with carboxylate moieties but also with

ether functionalities. The greatest C—H···O association energies belong to cooperative interactions, which as aforementioned in the introduction is a key role of C—H···O interactions. When combined with N—H$_{anti}$···O=C$_{isn}$, the C—H···O are biased towards the strong homo-synthon and are almost neglectable since interaction strengths of **1** and **2** are tantamount to the N—H···O associations in the 2-FA analogs, in which this contribution is missing. From previous works [19] is inferred that the chelating nature of 2-FA is valuable to promote DRST processes by increasing the coordination ability of the vicinal carboxylate O atom, but partakes in fewer interactions than its isomeric form 3-FA due to competition with the carboxylate O atom. Apart from the constrained O furane, the rest of the interactions follow Etter's rule so α and β values are capable of describing these interactions, which grants a certain degree of predictability. Among all the complexes, all those composed of Pip ligands present stronger C—H···O interactions with respect to those with 2-FA and 3-FA.

3.6. Photophysical properties

Aiming to study the behavior of complexes **1**–**4** in MeOH solutions, we measured their photophysical properties. To verify the non-aggregation of the ligands (S.I.: Figs. S19-S21) and complexes (S.I.: Figs. S22-S25), as well as avoiding aggregation-caused quenching of the fluorescence experiments [48], we performed additive measurements from $\sim 1 \times 10^{-9}$ M to $\sim 1 \times 10^{-4}$ M to observe the changes produced in the absorption spectra upon increasing the concentration. In addition, we have also provided comparative spectra of the ligands and their complexes at the concentrations utilized for the emission measurements (S.I.: Figs. S26 and S27). Relevant details about the photophysical properties of the ligands have been also supplied (S.I.: Table S4), while the corresponding information of the complexes is displayed in Table 7.

Table 7
Detailed parameters extracted from the photophysical properties of 1–5.

Compound	$\lambda_{max\text{-}abs}$ (log(ε))[a,b]	λ_{exc} [a]	$\lambda_{max\text{-}em}$ [a]	Stokes shift [c]	Φ_s [d]
1	201 (4.38), 223 (4.47), 275 (4.03)	230	312, 339	11,427, 13,980	0.01
2	202 (4.69), 226 (4.42), 269 (4.05)		314, 348	11,631, 14,743	0.02
3	202 (4.38), 222 (4.59), 274 (3.87)		309, 346	11,116, 14,577	0.17
4	201 (4.45), 223 (4.36), 271 (3.72)		310, 345	11,220, 14,493	0.70

[a] All the wavelengths are given in nm. $\lambda_{max\text{-}abs}$ = maximum of absorption; λ_{exc} = excitation maximum; $\lambda_{max\text{-}em}$ = maximum of emission. [b] ε values are given in M^{-1} × cm^{-1}. [c] Stokes shift are given in cm^{-1}. [d] Φ_s = relative quantum yield of the samples using L-tyr as the standard (Φ = 0.14) [49].

Compounds **1**–**4** presented three bands around ∼202 nm, ∼223 nm and ∼270 nm. The resulting additive spectra do not show significant changes below ∼1 × 10^{-7} M. Upon concentration, the bands around ∼270 nm showed hypsochromic (**1** and **2**) and bathochromic (**3** and **4**) shifts, suggesting the formation of H- and J-aggregates, respectively [50]. Thus, we decided to analyze the photophysical properties using solutions of ∼1 × 10^{-8} M, observing the **4** < **1** < **2** < **3** order of absorption intensity (S.I.: Fig. S27). Comparing the absorption spectra of **1**–**4** with analogous complexes bearing isn and 4-acpy [15,19], we tentatively attributed their transitions to be mainly ligand centered (LC) over the 3-FA ligand, with minor contributions of the pyridine ligands (S.I.: Figs. S28-S31), where isn should promote intra-ligand charge transfers (ILCT), and 4-acpy should display local excitations over the 4-acpy due to the disposition of these ligands in the paddle-wheel motif of **3**, or mixtures of LC transitions between the components of **4**.

Fluorescence measurements from all the compounds were done using the ∼1 × 10^{-8} M solutions utilized in the absorption measurements, and they were excited at λ_{exc} = 230 nm. The resulting emission spectra showed unfolded bands with two apparent peaks centered around 312 and 339 nm (**1**), 314 and 348 nm (**2**), 309 and 346 nm (**3**), and 310 and 345 nm (**4**) with intensities following the **4** < **1** < **3** < **2** order (Table 7, Fig. 9). The emission of compounds **1**–**4** displayed hypsochromic shifts compared with their former ligands (S.I.: Table S4, Figs. S32-S35). Moreover, the colors obtained according to the CIE 1931 chromaticity diagram are blue (**1**) and electric violet (**2**–**4**) (S.I.: Fig. S36).

The relative quantum yields (Φ_s) of **1**–**4** have been calculated using 1.01 × 10^{-7} M solutions of L-tyrosine in Milli-Q water as reference (Φ_{ref} = 0.14) [49], and Eq. (1):

$$\Phi_s = \Phi_{ref} \times \left(\frac{OD_{ref}}{OD_s}\right) \times \left(\frac{I_s}{I_{ref}}\right) \times \left(\frac{n_s}{n_{ref}}\right)^2 \qquad \text{Eq. (1)}$$

where OD is the optical density (or absorbance) at the selected excitation wavelength, I is the area under the curve of the emission spectra, and n is the refractive index of the solvents at 298 K [51]. The resulting Φ_s are 0.01 (**1**), 0.02 (**2**), 0.17 (**3**), and 0.70 (**4**) (Table 7). The Φ_s of **1** and **2** are lower than those of **3** and **4**, which could be attributed to the probable rotation in solution of the isn ligands in the dimeric scaffold towards the formation of intramolecular interactions, which resulted in charge transfer quenching mechanisms [52]. Besides, it seems that the bigger size of Cd(II) respect Zn(II) also influenced the Φ_s values, which could be related to quenching mechanisms by steric crowding effects around the metal *cores* [53,54].

4. Conclusions

We have successfully synthesized and characterized four Zn(II)/Cd(II) compounds containing 3-FA and two different dPy (isn and 4-acpy). Compounds **1** and **2** consisted in two isostructural complexes containing isn, which directed the dimeric motif due to their amide···amide homosynthons. Otherwise, compounds containing 4-acpy lead to a Zn(II) paddle-wheel (**3**) and a Cd(II) monomer (**4**) presenting 4-acpy, which does not provide any directional supramolecular interactions. The coordination modes of the 3-FA ligand displayed different behavior (μ_2-η^2 and μ_2-η^1: η^1), while the coordination numbers of the complexes oscillate between five and seven. Despite being weaker than conventional hydrogen bonds, C—H···O interactions demonstrated a guiding nature that follows Etter's rule and provides a certain degree of predictability. It has been inferred that C—H···O interactions implying carboxylate functional groups are crucial in the arrangement of metal carboxylate complexes with dPy. Besides, the role of ether functionalities in C—H···O interactions seems to be mainly associated with cooperativity for less donor C—H groups, but achieving significant interaction energies that strongly contribute to the supramolecular
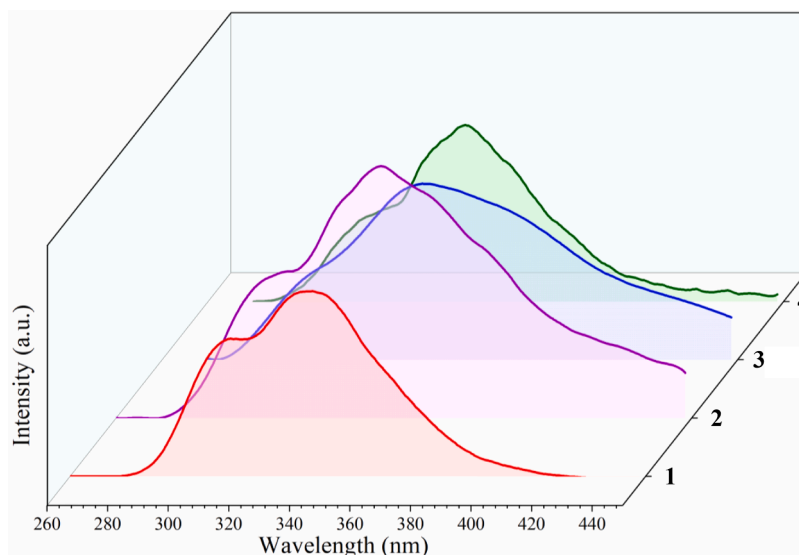
Fig. 9. Emission spectra of complexes **1**–**4** excited at 230 nm using MeOH solution of ∼1 × 10^{-8} M.

structure. Interestingly, the studied carboxylic acid C—H donors follow the order 3-FA $\simeq$ 2-FA > HPip from the calculated α values while HPip is the best O ether-acceptor, and indeed, the greatest interaction energies implying ether groups originate from Pip complexes. Finally, the photophysical properties of **1**–**4** have been measured in MeOH solutions observing better Φ_S values for compounds containing 4-acpy (**3** and **4**) compared with those with isn (**1** and **2**), which we attributed to: (i) the disruption of the amide···amide homosynthons of the isn moieties in solution for **1** and **2** causing quenching mechanisms of fluorescence and (ii) the different size of Zn(II) respect Cd(II) which allow avoiding steric crowding effects for the Cd(II) complexes.

CRediT authorship contribution statement

Francisco Sánchez-Férez: Data curation, Formal analysis, Investigation, Methodology, Software, Visualization, Writing – original draft. **Daniel Ejarque:** Data curation, Formal analysis, Investigation, Methodology, Software, Visualization, Writing – original draft. **Teresa Calvet:** Resources, Validation. **Mercè Font-Bardia:** Data curation, Formal analysis. **Josefina Pons:** Conceptualization, Funding acquisition, Project administration, Resources, Supervision, Validation, Writing – review & editing.

Declaration of competing interest

The authors declare that they have no known competing financial interests or personal relationships that could have appeared to influence the work reported in this paper.

Data availability

Data will be made available on request.

Acknowledgements

Supplementary materials

Supplementary material associated with this article can be found, in the online version, at doi:10.1016/j.molstruc.2024.138206.

Appendix A. Supplementary data

CCDC numbers 2324356 (**1**), 2324355 (**2**), 2324353 (**3**), and 2324354 (**4**) contain the supplementary crystallographic data for this paper. These data can be obtained free of charge via www.ccdc.cam.ac.uk/data_request/cif, or by emailing data_request@ccdc.cam.ac. uk, or by contacting The Cambridge Crystallographic Data centre, 12 Union Road, Cambridge CB2 1EZ, UK; fax: +44 1223 336,033.

References

[1] D. June Sutor, The C–H… O hydrogen bond in crystals, Nature 195 (1962) 68–69, https://doi.org/10.1038/195068a0.

[2] R. Taylor, O. Kennard, Crystallographic evidence for the existence of CH···O, CH···N and CH···Cl hydrogen bonds, J. Am. Chem. Soc. 104 (1982) 5063–5070, https://doi.org/10.1021/ja00383a012.

[3] Y. Mandel-Gutfreund, H. Margalit, R.L. Jernigan, V.B. Zhurkin, A role for CH…O interactions in protein-DNA recognition, J. Mol. Biol. 277 (1998) 1129–1140, https://doi.org/10.1006/jmbi.1998.1660.

[4] A.C. Pierce, K.L. Sandretto, G.W. Bemis, Kinase inhibitors and the case for CH…O hydrogen bonds in protein–ligand binding, Proteins 49 (2002) 567–576, https://doi.org/10.1002/prot.10259.

[5] L. Jiang, L. Lai, CH···O hydrogen bonds at protein-protein interfaces, J. Biol. Chem. 277 (2002) 37732–37740, https://doi.org/10.1074/jbc.M204514200.

[6] G.R. Desiraju, C–H···O and other weak hydrogen bonds. From crystal engineering to virtual screening, Chem. Commun. (2005) 2995, https://doi.org/10.1039/b504372g.

[7] G.R. Desiraju, DESIRAJU: C-H···O hydrogen bonding and the deliberate design of organic crystal structures, Mol. Cryst. Liq. Cryst. Sci. Technol. Sect. A. Mol. Cryst. Liq. Cryst. 211 (1992) 63–74, https://doi.org/10.1080/10587259208025806.

[8] F. Biedermann, H.J. Schneider, Experimental binding energies in supramolecular complexes, Chem. Rev. 116 (2016) 5216–5300, https://doi.org/10.1021/acs.chemrev.5b00583.

[9] W. Ji, G. Liu, Z. Li, C. Feng, Influence of C–H···O hydrogen bonds on macroscopic properties of supramolecular assembly, ACS Appl. Mater. Interfaces 8 (2016) 5188–5195, https://doi.org/10.1021/acsami.6b00580.

[10] A.N. Campbell, E.M. Kartzmark, The energy of hydrogen bonding in the system: acetone–bromoform, Can. J. Chem. 44 (1966) 917–924, https://doi.org/10.1139/v66-134.

[11] S. Pullanchery, S. Kulik, B. Rehl, A. Hassanali, S. Roke, Charge transfer across C–H···O hydrogen bonds stabilize oil droplets in water, Science 374 (2021) 1366–1370, https://doi.org/10.1126/science.abj3007.

[12] R. Taylor, It Isn't, It Is: the C–H···X (X = O, N, F, Cl) interaction really is significant in crystal packing, Cryst. Growth Des. 16 (2016) 4165–4168, https://doi.org/10.1021/acs.cgd.6b00736.

[13] J. Czernek, J. Brus, V. Czerneková, L. Kobera, Quantifying the intrinsic strength of C–H···O intermolecular interactions, Molecules 28 (2023) 4478, https://doi.org/10.3390/molecules28114478.

[14] K.B. Moore, K. Sadeghian, C.D. Sherrill, C. Ochsenfeld, H.F. Schaefer, C–H···O Hydrogen Bonding, The prototypical methane-formaldehyde system: a critical assessment, J. Chem. Theory Comput. 13 (2017) 5379–5395, https://doi.org/10.1021/acs.jctc.7b00753.

[15] F. Sánchez-Férez, J.M. Rius-Bartra, J.A. Ayllón, T. Calvet, M. Font-Bardia, J. Pons, Tuning photophysical properties by p-functional groups in Zn(II) and Cd(II) Complexes with piperonylic acid, Molecules 27 (2022) 1365.

[16] D. Ejarque, F. Sánchez-Férez, J.A. Ayllón, T. Calvet, M. Font-Bardia, J. Pons, Diverse structures and dimensionalities in Zn(II), Cd(II), and Hg(II) metal complexes with piperonylic acid, Cryst. Growth Des 20 (2020) 383–400.

[17] C.P. Li, M. Du, Role of solvents in coordination supramolecular systems, Chem. Commun. 47 (2011) 5958, https://doi.org/10.1039/c1cc10935a.

[18] W. Wang, Y.X. Wang, H.B. Yang, Supramolecular transformations within discrete coordination-driven supramolecular architectures, Chem. Soc. Rev. 45 (2016) 2656–2693, https://doi.org/10.1039/C5CS00301F.

[19] D. Ejarque, F. Sánchez-Férez, N. Félez-Guerrero, T. Calvet, M. Font-Bardia, J. Pons, Pyridine-driven assembly of Zn(ii) and Cd(ii) complexes with 2-furoic acid. The role of water in a structural transformation, CrystEngComm 25 (2023) 2739–2754, https://doi.org/10.1039/d3ce00104k.

[20] G.M. Sheldrick, A short history of SHELX, Acta Crystallogr. A. 64 (2008) 112–122, https://doi.org/10.1107/S0108767307043930.

[21] M.J. Frisch, G.W. Trucks, H.B. Schlegel, G.E. Scuseria, M.A. Robb, J.R. Cheeseman, G. Scalmani, V. Barone, G.A. Petersson, H. Nakatsuji, X. Li, M. Caricato, A. Marenich, J. Bloino, B.G. Janesko, R. Gomperts, B. Mennucci, H.P. Hratchian, J. V. Ortiz, A.F. Izmaylov, J.L. Sonnenberg, D. Williams-Young, F. Ding, F. Lipparini, F. Egidi, J. Goings, B. peng, A. Petrone, T. Henderson, D. Ranasinghe, V. G. Zakrzewski, J. Gao, N. Rega, G. Zheng, W. Liang, M. Hada, M. Ehara, K. Toyota, R. Fukuda, J. Hasegawa, M. Ishida, T. Nakajima, Y. Honda, O. Kitao, H. Nakai, T. Vreven, K. Throssell, J.A. Montgomery Jr., J.E. Peralta, F. Ogliaro, M. Bearpark, J.J. Heyd, E. Brothers, K.N. Kudin, V.N. Staroverov, T. Keith, R. Kobayashi, J. Normand, K. Raghavachari, A. Rendell, J.C. Burant, S.S. Iyengar, J. Tomasi, M. Cossi, J.M. Milliam, M. Klene, C. Adamo, R. Cammi, J.W. Ochterski, R.L. Martin, K. Morokuma, O. Farkas, J.B. Foresman, D.J. Fox, Gaussian 09, Revision D.01, Gaussian, Inc., Wallingford CT, 2016.

[22] W.J. Hehre, K. Ditchfield, J.A. Pople, Self-consistent molecular orbital methods. XII. further extensions of gaussian-type basis sets for use in molecular orbital studies of organic molecules, J. Chem. Phys. 56 (1972) 2257–2261.

[23] M.M. Francl, W.J. Pietro, W.J. Hehre, J.S. Binkley, M.S. Gordon, D.J. DeFrees, J. A. Pople, Self-consistent molecular orbital methods. XXIII. A polarization-type basis set for second-row elements, J. Chem. Phys. 77 (1982) 3654–3665.

[24] D. Musumeci, C.A. Hunter, R. Prohens, S. Scuderi, J.F. McCabe, Virtual cocrystal screening, Chem. Sci. 2 (2011) 883, https://doi.org/10.1039/c0sc00555j.

[25] T. Lu, F. Chen, Multiwfn: a multifunctional wavefunction analyzer, J. Comput. Chem. 33 (2012) 580–592.

[26] W. Humphrey, A. Dalke, K. Schulten, VMD: visual molecular dynamics, J. Mol. Graph. 14 (1996) 33–38, https://doi.org/10.1016/0263-7855(96)00018-5.

[27] D. Jayatilaka, D.J. Grimwood, Tonto: a fortran based object-oriented system for quantum chemistry and crystallography, Computational Science - ICCS; P.M.A. Sloot; D. Abramon; A.V. Bogdanov; J.J. Dongarra; A.Y. Zomaya; Y.E. Gorbachev. Eds.; 2003, 4, 142–151. https://doi.org/10.1007/3-540-44864-0_15.

[28] M.J. Turner, J.J. McKinnon, S.K. Wolff, D.J. Grimwood, P.R. Spackman, D. Jayatilaka, M.A. Spackman, CrystalExplorer17, 2017. http://hirshfeldsurface.net.

[29] C.F. Mackenzie, P.R. Spackman, D. Jayatilaka, M.A. Spackman, CrystalExplorer model energies and energy frameworks: extension to metal coordination compounds, organic salts, solvates and open-shell systems, IUCrJ 4 (2017) 575–587, https://doi.org/10.1107/S205225251700848X.

[30] P.R. Spackman, M.J. Turner, J.J. McKinnon, S.K. Wolff, D.J. Grimwood, D. Jayatilaka, M.A. Spackman, CrystalExplorer : a program for Hirshfeld surface analysis, visualization and quantitative analysis of molecular crystals, J. Appl. Crystallogr. 54 (2021) 1006–1011, https://doi.org/10.1107/S1600576721002910.

[31] S.P. Thomas, P.R. Spackman, D. Jayatilaka, M.A. Spackman, Accurate lattice energies for molecular crystals from experimental crystal structures, J. Chem. Theory Comput. 14 (2018) 1614–1623, https://doi.org/10.1021/acs.jctc.7b01200.

[32] Y. Ji, X. Yang, Z. Ji, L. Zhu, N. Ma, D. Chen, X. Jia, J. Tang, Y. Cao, DFT-calculated IR spectrum amide I, II, and III band contributions of N -methylacetamide fine components, ACS Omega 5 (2020) 8572–8578, https://doi.org/10.1021/acsomega.9b04421.

[33] G.B. Deacon, Relationships between the carbon-oxygen stretching frequencies of carboxylato complexes and the type of carboxylate coordination, Coord. Chem. Rev. 33 (1980) 227–250, https://doi.org/10.1016/S0010-8545(00)80455-5.

[34] I. Fleming, D. Williams, Spectroscopic Methods in Organic Chemistry, 7th ed., Springer International Publishing, Cham, 2008 https://doi.org/10.1007/978-3-030-18252-6.

[35] J. Cepeda, S. Pérez-Yáñez, J.Á. García, S. Rojas, A. Rodríguez-Diéguez, Towards correlating dimensionality and topology in luminescent MOFs based on terephthalato and bispyridyl-like ligands, Dalton Trans. 50 (2021) 9269–9282, https://doi.org/10.1039/D1DT01204E.

[36] M. Llunell, D. Casanova, J. Cirera, P. Alemany, S. Alvarez, SHAPE. Program for the Stereochemical Analysis of Molecular Fragments by Means of Continuous Shape Measures and Associated Tools, Universitat de Barcelona, Barcelona, 2013.

[37] M. Pinsky, D. Avnir, Continuous Symmetry Measures. 5. The Classical Polyhedra, 37, Inorg, Chem, 1998, pp. 5575–5582, https://doi.org/10.1021/ic9804925.

[38] D. Chisca, L. Croitor, O. Petuhov, O.V. Kulikova, G.F. Volodina, E.B. Coropceanu, A.E. Masunov, M.S. Fonari, Tuning structures and emissive properties in a series of Zn(II) and Cd(II) coordination polymers containing dicarboxylic acids and nicotinamide pillars, CrystEngComm 20 (2018) 432–447, https://doi.org/10.1039/C7CE01988B.

[39] V. Lozovan, V.C. Kravtsov, E.B. Coropceanu, N. Siminel, O.V. Kulikova, N. V. Costriucova, M.S. Fonari, Seven Zn(II) and Cd(II) 1D coordination polymers based on azine donor linkers and decorated with 2-thiophenecarboxylate: syntheses, structural parallels, Hirshfeld surface analysis, and spectroscopic and inclusion properties, Polyhedron 188 (2020) 114702, https://doi.org/10.1016/j.poly.2020.114702.

[40] A. Karmakar, R.J. Sarma, J.B. Baruah, Self-assembly of neutral dinuclear and trinuclear zinc-benzoate complexes, Inorg. Chem. Commun. 9 (2006) 1169–1172, https://doi.org/10.1016/j.inoche.2006.07.013.

[41] L. Moreno-Gómez, F. Sánchez-Férez, T. Calvet, M. Font-Bardia, J. Pons, Zn(II) and Cd(II) monomer, dimer and polymer compounds coordinated by benzoic acid and 4-acetylpyridine: synthesis and crystal structures, Inorg. Chim. Acta 506 (2020) 119561, https://doi.org/10.1016/j.ica.2020.119561.

[42] E. Cimen, I. Gumus, O. Celik, E. Keskin, H. Arslan, Preparation, characterization and crystal structure of dinuclear zinc(II) carboxylate complex with 1-(pyridin-4-yl)ethanone and 4-methylbenzoate based ligands, Eur. J. Chem. 7 (2016) 448–453, https://doi.org/10.5155/eurjchem.7.4.448-453.1509.

[43] T. Hökelek, F. Yılmaz, B. Tercan, F. Gürgen, H. Necefoğlu, Aquabis(4-formylbenzoato-κ²O¹, O¹')bis(isonicotinamide-κN¹)cadmium(II) monohydrate, Acta Crystallogr. E65 (2009) m1416–m1417, https://doi.org/10.1107/S1600536809042640.

[44] A.S. Mahadevi, G.N. Sastry, Cooperativity in noncovalent interactions, Chem. Rev. 116 (2016) 2775–2825, https://doi.org/10.1021/cr500344e.

[45] S. Soudani, M. Hajji, J.X. Mi, C. Jelsch, F. Lefebvre, T. Guerfel, C.Ben Nasr, Synthesis, structure and theoretical simulation of a zinc(II) coordination complex with 2,3-pyridinedicarboxylate, J. Mol. Struct. 1199 (2020) 127015, https://doi.org/10.1016/j.molstruc.2019.127015.

[46] M.C. Etter, Encoding and decoding hydrogen-bond patterns of organic compounds, Acc. Chem. Res. 23 (1990) 120–126, https://doi.org/10.1021/ar00172a005.

[47] M.C. Etter, Hydrogen bonds as design elements in organic chemistry, J. Phys. Chem. 95 (1991) 4601–4610, https://doi.org/10.1021/j100165a007.

[48] P. Li, D. Zhang, Y. Zhang, W. Lu, J. Zhang, W. Wang, Q. He, P. Théato, T. Chen, Aggregation-caused quenching-type naphthalimide fluorophores grafted and ionized in a 3d polymeric hydrogel network for highly fluorescent and locally tunable emission, ACS Macro Lett. 8 (2019) 937–942, https://doi.org/10.1021/acsmacrolett.9b00337.

[49] R.F. Chen, Fluorescence quantum yields of tryptophan and tyrosine, Anal. Lett. 1 (1967) 35–42, https://doi.org/10.1080/00032716708051097.

[50] N.J. Hestand, F.C. Spano, Expanded theory of H- and J-molecular aggregates: the effects of vibronic coupling and intermolecular charge transfer, Chem. Rev. 118 (2018) 7069–7163, https://doi.org/10.1021/acs.chemrev.7b00581.

[51] G.M. Hale, M.R. Querry, Optical constants of water in the 200-nm to 200-μm wavelength region, Appl. Opt. 12 (1973) 555–563, https://doi.org/10.1364/AO.12.000555.

[52] P.L. Muiño, P.R. Callis, Solvent effects on the fluorescence quenching of tryptophan by amides via electron transfer. experimental and computational studies, J. Phys. Chem. B. 113 (2009) 2572–2577, https://doi.org/10.1021/jp711513b.

[53] N.J. Williams, W. Gan, J.H. Reibenspies, R.D. Hancock, Possible steric control of the relative strength of chelation enhanced fluorescence for zinc(II) compared to cadmium(II): metal ion complexing properties of tris(2-quinolylmethyl)amine, a crystallographic, UV-visible, and fluorometric study, Inorg. Chem. 48 (2009) 1407–1415, https://doi.org/10.1021/ic801403s.

[54] D. Ejarque, T. Calvet, M. Font-Bardia, J. Pons, Steric crowding of a series of pyridine based ligands influencing the photophysical properties of Zn(II) complexes, CrystEngComm 23 (2021) 6199–6213, https://doi.org/10.1039/D1CE00833A.